Cocrystallization of a Poly(ethylene−butene) Random Copolymer with C_{24} in *n*-Decane

Dietmar Schwahn and Dieter Richter*

Institute of Solid State Research, Research Center, Jülich, D-52425 Jülich, Germany

Min Lin

Center for Neutron Research, National Institute of Science and Technology, Gaithersburg, Maryland 20899-8562

Lewis J. Fetters†

Corporate Strategic Laboratories, Exxon Mobile Research and Engineering Company, Annandale, New Jersey 08801

Received November 26, 2001; Revised Manuscript Received February 4, 2002

ABSTRACT: Amorphous−crystalline random copolymers containing ethylene and butene (PEB) segments are known to self-assemble in solution to yield one-dimensional micellar structures, i.e., rodlike aggregates. This behavior stands in contrast with the amorphous−crystalline diblock polymers, where self-assembly leads to a core consisting of a rough textured plate of polyethylene cloaked by the amorphous component; either alternating poly(ethylene−propylene) or random poly(ethylene−butene). These materials serve as nucleation platforms for wax crystal size control in commercial formulations for middle distillate fuels. Here, we present small-angle neutron-scattering results to evaluate the influence of C_{24} wax in the presence of the PEB random copolymer upon the self-assembly event. In stark contrast to the rodlike micelles the random copolymers cocrystallize with the wax in thin sheets consisting of a single paraffin layer surrounded by amorphous polymer hairs on both plate sides. Such structures have not been seen before. The polymer brush is well-defined, indicating a homogeneous distribution of the polymer in the wax-stabilized plate. It can be conjectured that this behavior may prove to be a viable mechanism regarding the development of flow improvers for waxy crude stocks.

I. Introduction

Recent investigations have shown that wax crystal modifiers based on polyethylene−poly(ethylene−propylene) (PE−PEP) diblock copolymers function as nucleators for wax crystal size control in middle distillate fuels.[1,2] This diblock copolymer has also shown, on the laboratory scale, the capacity to serve as a flow improver in waxy crude oils.[3] These materials undergo self-assembly to yield plate structures[1] that in turn serve as wax crystal nucleation platforms by providing large PE surface areas.[2] They self-assemble to form expansive aggregates consisting of a PE core cloaked behind the amorphous PEP brush layer. The PE plate thus promotes nucleation of solubilized long chain paraffins. The thermodynamics of the diblock copolymer aggregation to hairy platelets has been described in terms of a free energy function based on the structural data obtained from small-angle neutron scattering (SANS).[2] From these results, it may be assumed that other wax crystal modifiers function on the basis of polymer aggregation, where the micelles act as nucleation sites.

This behavior invites the evaluation of other polymer architectures where semicrystalline and amorphous segments are combined in an alternating manner. Candidate structures include copolymers, where the composition variation signals the alteration between semicrystalline and amorphous segments. One such family are nearly random copolymers of ethylene and 1-butene; the PEB-*n* systems where *n* is the number of ethyl-groups/100 backbone carbons.[4,5] These materials, in the bulk, retain a crystalline melting point up to about $n = 14$.[5]

In this manuscript, we report on a series of experiments, where we studied the cocrystallization behavior of PEB-11 together with linear C_{24} in decane solution. In contrast to the PE−PEP diblock PEB-11 self-assembles in open rodlike structures.[6] While for the diblock copolymer the self-assembly occurs around 60 °C, the PEB-11 system shows the first signs of self-assembly only below 0 °C.

After a description of the sample synthesis and characterization, we briefly present some basic features of small-angle neutron scattering emphasizing the contrast variation approach. Thereafter, experimental results under different contrast and different wax-to-polymer ratios are presented for a wide range of temperatures. From these results a picture of wax−copolymer cocrystallization evolves, where at low wax-to-polymer ratios large combined wax−polymer platelets dominate, in which, for wax surplus, these plates appear to serve as nucleation templates for three-dimensional wax crystal growth.

II. Experimental Section

A. Synthesis and Characterization. The PEB materials were made in cyclohexane from either hydrogenous or perdeuterated 1,3-butadiene using standard anionic polymerization techniques.[7] Following synthesis, the samples were then saturated with hydrogen. The palladium on barium sulfate system was used. H NMR (*h*-polybutadiene) or C NMR

† Present address: School of Chemical Engineering, Cornell University, Ithaca, NY 14853.

10.1021/ma0120456 CCC: $22.00
Published on Web 03/27/2002

Table 1. Molecular Characteristics and Scattering Properties of the Chemicals Investigated

	h-PEB-11	*d*,*h*-PEB-11	*h*-tetracosane	*d*-tetracosane	*h*-decane	*d*-decane
M_w (g/mol)	400	6400	338	388	142	164
M_w/M_n	1.02	1.02			1	1
ζ (g/cm^3)	0.856	0.92	0.80	0.92	0.73	0.84
M_0 (g/mol)	17.2	18.49	338	388	142	164
V_0 (cm^3/mol)	20.08	20.08	422.5	422.5	194.5	194.5
ρ (10^{10} cm^{-2})	−0.31	3.72	−0.39	7.04	−0.49	6.58

Table 2. Microstructure of PEB-11[a]

triads	EEE	EEB + BEE	EBE	EBB + BBE	BEB	BBB
	0.46	0.32	0.13	0.09	0	0
diads	EE	EB + BE	BB	r_1r_2	cluster index	
	0.62	0.34	0.045	1	10.5	

[a] E: ethylene, B: butene. EEE and EE are percentages of ethylene triads and diads; similarly, EEB denotes ethylene−ethylene−butene triads and so on. r_1r_2 = the product of the reactivity ratios where convention dictates that r_1 refers to the majority monomer (in this case ethylene), the cluster index is a measure of randomness, where 10 is perfectly random. The PEB polymers cannot be perfectly random since BEB triads are not possible.

(*d*-polybutadiene) was used for microstructure analysis. The PEB copolymers contained 11 ethyl branches per 100 backbone carbon atoms. Table 1 displays the molecular characteristics. The hydrogenous and the deuterated versions of *n*-C_{24} were used in conjunction with these *h*-PEB and *d*,*h*-PEB samples. Size exclusion chromatography was used for the parent polybutadiene molecular characterizations. Both samples had molecular weights of 6.4 K and polydispersities no greater than 1.02. The sequence distributions of the *h*-PEB-11 are given in Table 2. The cluster index of nearly 10 demonstrates that the PEB-11 samples are virtually random copolymers. Parenthetically it should be mentioned that the BEB triad is not possible in these PEB copolymers since each parent 1,4 structure yields two ethylene units.

B. Neutron Small-Angle Scattering (SANS). The small-angle scattering of neutrons arises from the fluctuations of the scattering length densities within a material $\rho_i = (\sum b_i)/v_i$ where b_i are the scattering lengths of the different atoms in a monomer or molecule i and v_i is the volume of the corresponding entity. Under the assumption of incompressibility and with the definition of one of the molecular species as reference, its scattering length density may be noted by ρ_s. The coherent cross section per volume is then given by

$$I(\underline{Q}) = \sum_{ij}(\rho_i - \rho_s)(\rho_j - \rho_s)P_{ij}(\underline{Q}) \quad (1)$$

With the partial structure factors, $P_{ij}(\underline{Q})$

$$P_{ij}(\underline{Q}) = \frac{1}{V_S}\int\langle\phi_i(\underline{r})\phi_j(\underline{r'})\exp(i\underline{Q}(\underline{r}-\underline{r'}))\,\mathrm{d}^3\underline{r}\,\mathrm{d}^3\underline{r'}\rangle \quad (2)$$

The integration is performed over the sample volume V_S and $\phi_i(\underline{r})$ describes the volume fraction of monomer or molecule i at a position r. $|\underline{Q}| = (4\pi/\lambda)\sin(\theta/2)$ is the scattering wavenumber with θ the scattering angle and λ the neutron wavelength. For a ternary system containing oil, polymer and paraffin and using oil as a reference, the scattering intensity is usually isotropic and may be described in terms of partial structure factors as

$$I(Q) = (\rho_p - \rho_s)^2P_{pp}(Q) + 2(\rho_p - \rho_s)(\rho_w - \rho_s)P_{pw}(Q) + (\rho_w - \rho_s)^2P_{ww}(Q) \quad (3)$$

where p and w indicate here polymer and wax (paraffin), respectively. For a noninteracting system $P_{pp}(Q)$ relates to the microscopic structure of a single chain.

A detailed SANS study of the structures formed by the polymer paraffin mixtures at decreasing temperatures requires the contrast matching technique which concerns the variation of the degree of hydrogenation or deuteration of the different components of the sample. In this way, in eq 3 all but one partial structure factor may be made invisible. For the polymer solutions in decane, the maximum contrast is achieved using fully protonated polymers in a fully deuterated solvent.

Decreasing the temperature, the self-assembly of polymers and paraffin, or common aggregation processes results in the formation of large objects with a characteristic morphology for each of the investigated systems. The scattering from these objects may often be characterized by power laws

$$I(Q) \approx Q^{-\alpha} \quad (4)$$

where the exponent α signifies the spatial arrangements of the polymers and paraffin, respectively.

The objects resulting from the aggregation process may assume different shapes like rods, platelets, and so on. The scattering from a rodlike structure is characterized by an exponent $\alpha = 1$ in eq 4. Using the Guinier approximation, the cross section for such aggregates has the form

$$\frac{\mathrm{d}\Sigma}{\mathrm{d}\Omega}(Q) = \phi_{rod}(1-\phi_{rod})\pi F_{rod}\Delta\rho^2\exp(-Q^2a^2/4)/Q \quad (5)$$

where $F_{rod} = \pi a^2$ is the perpendicular area of the rod, a the rod radius, and ϕ_{rod} the volume fraction of rods. Note, for rods partially swollen with solvent, $\Delta\rho$ is now the contrast between the polymer plus solvent within the rod relative to the solvent.

The scattering of platelets with constant thickness leads to a Q^{-2} power law. Here, the Guinier approximation has the following form

$$\frac{\mathrm{d}\Sigma}{\mathrm{d}\Omega}(Q) = \phi_{plate}(1-\phi_{plate})\Delta\rho^2 2\pi d_{eff}\exp(-Q^2d_{eff}^2/12)/Q^2 \quad (6)$$

where d_{eff} is the plate thickness and ϕ_{plate} the volume fraction of the plates. For $\Delta\rho$ the same remark holds as before.

Aggregates representing 3-dimensional large objects with sharp interfaces and $QR_g \gg 1$ give rise to Porod scattering.

$$\frac{\mathrm{d}\Sigma}{\mathrm{d}\Omega}(Q) = \phi_{agg}2\pi\Delta\rho^2(S/V)Q^{-4} = P_4Q^{-4} \quad (7)$$

where S is the surface and V the volume of the aggregates. Exponents $\alpha < 3$ and $3 < \alpha < 4$ in eq 4 relate to mass or surface fractals respectively, while $\alpha > 4$ is characteristic for diffuse interfaces.

C. SANS Experiments. For the small-angle scattering experiments, a number of samples under different contrast matching conditions were prepared. In each case the polymer volume fraction was kept at $\phi_{pol} = 0.01$, while the volume fraction of wax was varied in three steps from $\phi_{wax} = 0.005$, $\phi_{wax} = 0.01$ to $\phi_{wax} = 0.02$. Polymer contrast was achieved [$(\rho_{wax} - \rho_{sol}) \approx 0$ in eq 3] using *h*-PEB-11 in deuterated decane with deuterated wax. To achieve wax contrast the dh PEB-11 was matched by a mixture of *h*- and *d*-decane and *h*-C_{24} was added. The contrast conditions and sample compositions are displayed in Table 3.

The small-angle neutron scattering (SANS) data were accumulated at the SANS facilities KWS-1 and KWS-2 at the FRJ-2 research reactor in Jülich, Germany and at NIST in Gaithersburg, Maryland.[8] The Q ranges were $0.0015 < Q < 0.14$ Å^{-1}. The data were corrected for the scattering from the

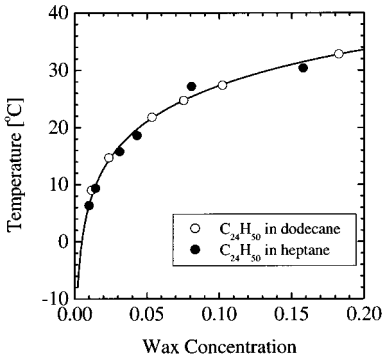

Figure 1. Dissolution line of $C_{24}H_{50}$ in short chain hydrocarbons: (○) $C_{24}H_{50}$ in dodecane; (●) $C_{24}H_{50}$ in heptane.[9]

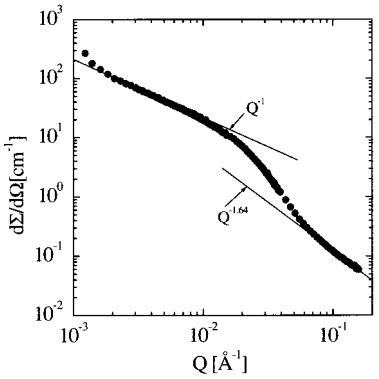

Figure 2. Absolute cross section of PEB-11 in decane at a volume fraction of $\phi_{pol} = 0.02$. The two solid lines indicate the asymptotic power law scattering behavior at low and high Q respectively. The corresponding exponents amount to $\alpha = 1$ and $\alpha = 1.64$, respectively.

Table 3. Sample Compositions and Cross Sections[a]

	sample 1	sample 2	sample 3	ample 4	sample 5	sample 6
ϕ(*h*-PEB-11)	**0.01**	**0.01**	**0.01**	0	0	0
ϕ(*h*,*d*-PEB-11)	0	0	0	0.01	0.01	0.01
ϕ(*h*-C_{24})	0	0	0	**0.05**	**0.01**	**0.02**
ϕ(*d*-C_{24})	0.005	0.01	0.02	0	0	0
% *h*-decane	0	0	0	40	40	40
ρ_s (10^{10}/cm^2)	6.58	6.58	6.58	3.72	3.72	3.72

[a] Bold numbers highlight the visible component.

empty cell and the background obtained from a Cd-run. Calibration to absolute intensities was performed by a water and Lupolen standard, respectively. Temperature control was achieved with a precision of $\delta T = \pm 1$ °C in measuring the temperature with a thermocouple in the sample cell. The phase diagrams of C_{24} in short hydrocarbons were determined recently by Brecevic and Garside.[9] The dissolution lines for C_{24} in heptane and dodecane are displayed in Figure 1 as a function of C_{24} volume fraction.

III. Results

We start by recalling the self-assembly properties of PEB-11 ($\phi_{pol} = 0.02$) in decane without wax.[6] Figure 2 shows the scattering profile of the PEB-11 at −30 °C, wherein it is seen that the mid- to low-Q data shows a gradient of $\alpha = -1$. This demonstrates the existence of a one-dimensional self-assembled structure (see eqs 4 and 5). Thus, contrary to the platelet structures seen previously for the PE−PEP diblocks, where the experimental gradient was $\alpha = -2$, at low Q, the $\alpha = -1$ value signifies a rodlike quasi-one-dimensional aggregate.[1,2]

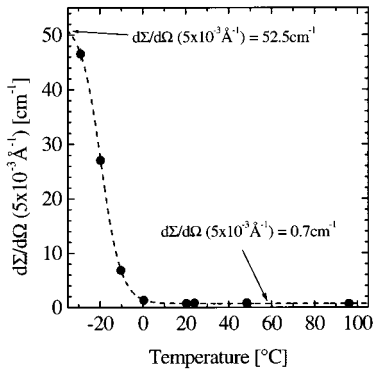

Figure 3. Temperature dependence of the aggregation related cross section from the PEB-11 solution. The cross sections are taken at $Q = 5 \times 10^{-3}$ Å^{-1}, and the dashed line serves as a guide to the eye.

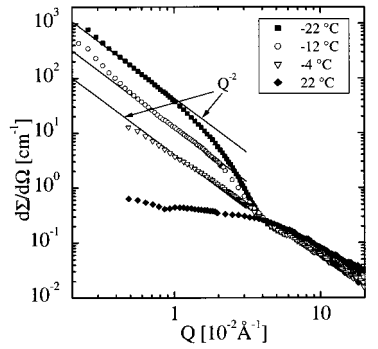

Figure 4. Small-angle scattering cross sections from a solution of PEB-11 ($\phi_{pol} = 0.01$) and C_{24} ($\phi_{wax} = 0.005$) in decane under polymer contrast (sample 1). The solid lines indicate the asymptotic Q^{-2} law.

Furthermore, we note in the limiting high Q regime a slope $\alpha = -1.64$ is found, which is indicative of swollen chains. As has been discussed in ref 6, the aggregates contain large fractions of solvent preserving locally the picture of a polymer solution. Figure 3 depicts the temperature evolution of the self-assembly event in displaying the measured cross section at $Q = 0.005$ Å^{-1}. At this Q, the intensity is sensitive to the occurrence of self-assembled structures. For temperatures above 0 °C single chain cross sections were observed. At $T = 0$ °C, the first weak evidence for a beginning aggregation process occurs while at −8 °C a robust signal of self-assembly becomes visible.

A. Observations under Polymer Contrast. Figure 4 presents temperature-dependent SANS pattern from the sample with the lowest wax content ($\phi_{wax} = 0.005$) where the wax was matched by the solvent (sample 1, Table 3). The difference to Figure 2, where the self-assembly of the polymer alone is displayed, is striking. A small addition of wax alters the polymer self-assembly completely which now features 2-d aggregate structures. This is demonstrated by the low-Q data at lower temperature, where $d\Sigma/d\Omega \sim Q^{-2}$ signifies plate scattering (see eq 6) instead that of rods (Q^{-1}). Thus, the presence of the wax changes the aggregation behavior of PEB-11 from rodlike to platelike structures. These platelike aggregates commence to appear first at −4 °C, while at 22 °C the single chain cross section is primarily visible. The data indicate that the wax is cocrystallizing with the PE segments of the random copolymer. Unlike the PE−PEP diblock, which in effect performs as a

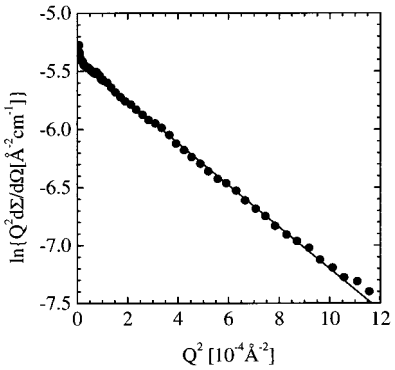

Figure 5. Small-angle scattering results from a solution of PEB-11 ($\phi_{pol} = 0.01$) and C_{24} ($\phi_{wax} = 0.005$) in decane in a Guinier presentation (eq 6) at $T = -22$ °C. The slope leads to a plate thickness of $d_{eff} = 147$ Å. The interception with $Q^2 = 0$ gives the forward scattering of $Q^2 d\Sigma/d\Omega$ ($Q = 0$) = (4.52 ± 0.02) × 10^{13} cm^{-3}.

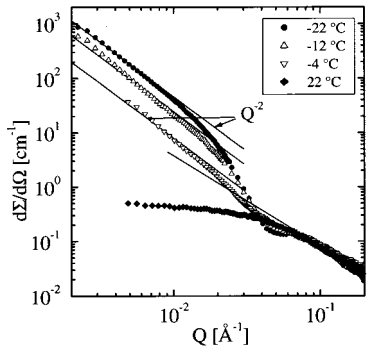

Figure 6. Small-angle scattering traces from a solution of PEB-11 ($\phi_{pol} = 0.01$) and C_{24} ($\phi_{wax} = 0.01$) in decane (sample 2) under polymer contrast at various temperatures. The solid lines indicate the asymptotic Q^{-2} law.

nucleation platform, the PEB-11 random copolymer has its self-assembly altered by the presence of wax.

In the Q regime above $Q \simeq 10^{-2}$ Å^{-1}, the scattering profile departs from the Q^{-2} asymptote in bending toward lower intensities. Obviously, the finite plate thickness becomes important. An evaluation in terms of the Guinier approximation (eq 5) yields the plate thickness $d_{eff} \simeq 147$ Å as well as the forward scattering (see Figure 5). Both values are tabulated in Table 4. Figures 6 and 7 display the corresponding scattering patterns for the higher wax volume fractions $\phi_{wax} = 0.01$ (sample 2) and $\phi_{wax} = 0.02$ (sample 3). In all cases, signatures of platelike aggregates are found. We note that at the lowest temperature ($T = -22$ °C) the observed forward scattering for the wax volume fractions is practically the same. The observed plate thicknesses are very close.

The scattering data of Figures 6 and 7, in particular at −22 °C, exhibit a well-defined minimum around $Q = 0.04$ Å^{-1}. From such a scattering profile the form factor of the plate may be evaluated. For an infinite

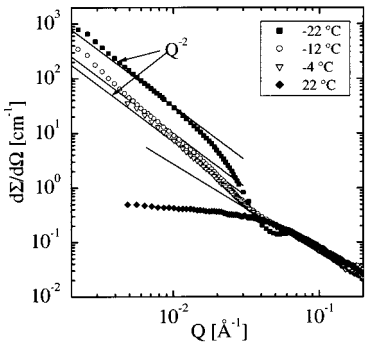

Figure 7. Small-angle scattering data from a solution of PEB-11 ($\phi_{pol} = 0.01$) and C_{24} ($\phi_{wax} = 0.02$) in decane (sample 3) under polymer contrast at various temperatures. The solid lines indicate the asymptotic Q^{-2} law.

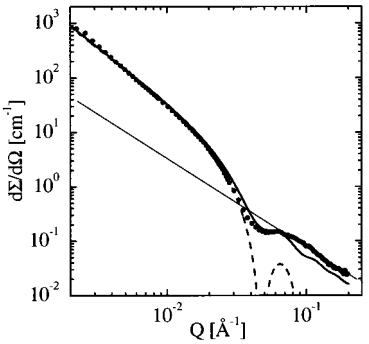

Figure 8. Fit of the small-angle scattering data from a solution of PEB-11 ($\phi_{pol} = 0.01$) and C_{24} ($\phi_{wax} = 0.02$) in decane (sample 3) under polymer contrast with the scattering cross section resulting from a combination of eq 9 and 6. The solid line results from a superposition of the aggregate scattering and the single chain contribution.

plate with a perpendicular density profile $C_p(z)$ the form factor is given by

$$P(Q) = \left| \int_{-\infty}^{+\infty} C_p(z) e^{iQz} \, dz \right|^2 \tag{8}$$

For a rectangular profile of width d_{eff} we have

$$P(Q) = \left(\sin\left(\frac{Q d_{eff}}{2}\right) / (Q d_{eff}/2) \right)^2 \tag{9}$$

When the exponential Guinier term in eq 6 was replaced by eq 9, the scattering profile at $T = -22$ °C and $\phi_{wax} = 0.02$ was fitted with this function. Figure 8 compares the obtained fit with the experimental data. The dashed line presents the form factor as given by eq 9. The solid line includes in addition the asymptotic diffuse scattering from the monomer correlations within the chains. A good fit evolves yielding $d_{eff} = 132$ Å, agreeing favorably with that of 149 Å which was based upon the Guinier approximation.

B. Measurements under Wax Contrast. To achieve wax contrast following eq 3 polymer and solvent scattering length densities need to be matched. This was

Table 4. Polymer Aggregation Characteristics in the Presence of Wax (Samples 1−3)

	$T = -22$ °C		$T = -12$ °C		$T = -4$ °C	
ϕ_{wax}	d_{eff} (Å)	$Q^2(d\Sigma/d\Omega)$ (10^{13} cm^{-3})	d_{eff} (Å)	$Q^2(d\Sigma/d\Omega)$ (10^{13} cm^{-3})	d_{eff} (Å)	$Q^2(d\Sigma/d\Omega)$ (10^{13} cm^{-3})
0.005	147 ± 0.4	4.52 ± 0.02	121 ± 2.3	1.89 ± 0.05	−	0.4 ± 0.05
0.01	149 ± 1	4.8 ± 0.03	133 ± 2	2.2 ± 0.06	88 ± 1	0.8 ± 0.1
0.02	149 ± 0.4	4.1 ± 0.05	100 ± 0.5	0.99 ± 0.04	87 ± 1	0.76 ± 0.05

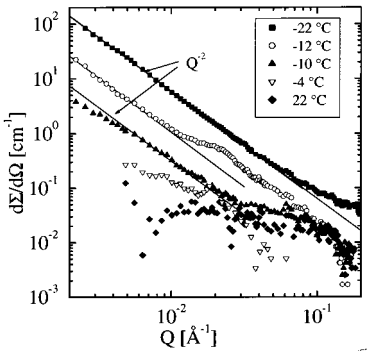

Figure 9. SANS results from a solution of PEB-11 ($\phi_{pol} = 0.01$) and C_{24} ($\phi_{wax} = 0.005$) in decane under wax contrast (sample 4). The solid lines indicate the Q^{-2} law.

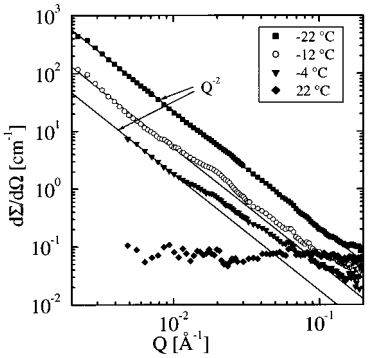

Figure 10. SANS results from a solution of PEB-11 ($\phi_{pol} = 0.01$) and C_{24} ($\phi_{wax} = 0.01$) in decane under wax contrast (sample 5). The solid lines indicate the Q^{-2}.

achieved using the partially deuterated *h,d*-PEB-11 in a mixture of deuterated and protonated decane (see Table 3) and employing hydrogenous wax. For the lowest wax volume fraction $\phi_{wax} = 0.005$ the temperature-dependent scattering profiles are displayed in Figure 9. The data displays a very pronounced Q^{-2} behavior up to high Q. From the cross section (eq 6), we are led to conclude that the plates need to be very thin since no bending away from the asymptotic Q^{-2} profile toward lower intensities is visible. The extended Q^{-2} pattern is compatible with plates from a single layer of stretched C_{24} molecules ($d_{eff} = 32$ Å) but excludes, e.g., stacks of two molecular layers. We note that already at −4 °C where according to the phase diagram all wax should be in solution some increase in the low-Q scattering is observed. The effect is even more pronounced at −10 °C. Figure 10 shows the 0.01 wax system, which yields scattering profiles very similar to that containing $\phi_{wax} = 0.005$ other than the intensities are significantly increased. Table 5 presents the obtained forward scattering as a function of temperature for both wax contents.

Figure 11 displays the SANS results for $\phi_{wax} = 0.02$, which differ qualitatively from the preceding date. Compared to the lower wax concentrations the scattering intensity is strongly enhanced and assumes a Q^{-4} power law at low Q indicative for the scattering from a well-defined surface of a 3-d object (see eq 7). The presence of this scattering profile suggests the presence of large 3-d wax crystals coexisting with platelike structures which still dominate the scattering pattern at higher Q. The scattering under polymer contrast from the same sample composition on the other hand relates always to 2-d structures. Decomposing the observed

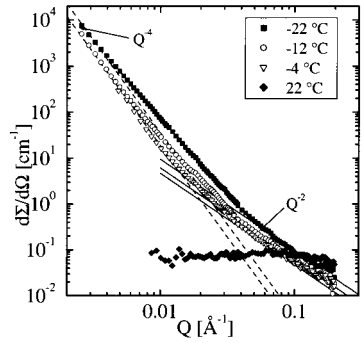

Figure 11. SANS results from a solution of PEB-11 ($\phi_{pol} = 0.01$) and C_{24} ($\phi_{wax} = 0.02$) in decane under wax contrast (sample 6). The solid lines indicate the asymptotic Q^{-2} law while the dashed lines present the Q^{-4} Porod scattering contribution.

Table 5. Wax Aggregation Characteristics in the Presence of Polymer (Samples 4−6)

ϕ_{wax}	$T = -22$ °C $Q^2(d\Sigma/d\Omega)$ (10^{13} cm^{-3})	$T = -12$ °C $Q^2(d\Sigma/d\Omega)$ (10^{13} cm^{-3})	$T = -4$ °C $Q^2(d\Sigma/d\Omega)$ (10^{13} cm^{-3})
0.005	0.68 ± 0.007	0.11 ± 0.015	0.03 ± 0.01
0.01	2.12 ± 0.02	0.5 ± 0.04	0.17 ± 0.03
0.02[a]	1.1 ± 0.1	0.75 ± 0.07	0.52 ± 0.05
ϕ_{wax}	P_4 (10^{25} cm^{-5})	P_4 (10^{25} cm^{-5})	P_4 (10^{25} cm^{-5})
0.02[a]	3.6	1.9	1.9

[a] Scattering from the plate contribution, Porod constant from the Q^{-4} part in the cross section.

intensities into contributions from platelet scattering eq 6 and Porod scattering (eq 7), we obtain Porod constants P_4 as well as the corresponding platelet caused forward scattering $Q^2 d\Sigma/d\Omega$. Both are given in Table 5.

IV. Interpretation and Discussion

We have found that the presence of C_{24} wax changes the aggregation behavior of PEB-11 from rod- to platelike structures. The wax plates are very thin and are in accordance with 2-d monolayer C_{24} wax crystals of 32 Å thickness. The polymer plate structures, on the other hand, are about five times as thick and are well described by a homogeneous polymer density distribution across the plates of narrow size distribution. The experimental finding strongly suggests a cocrystallization process, where wax and polymer jointly form platelet structures as is schematically indicated in Figure 12.

Starting from eq 6, we may further evaluate the aggregate structures. Considering the asymptotic forward scattering we have

$$\left.\frac{d\Sigma}{d\Omega}Q^2\right|_{wax} = \phi_{wax}^{plate}\Delta\rho_{wax}{}^2(\phi_{wax}^{layer})^2 2\pi d_{wax} \qquad (10a)$$

$$\left.\frac{d\Sigma}{d\Omega}Q^2\right|_{pol} = \phi_{pol}^{plate}\Delta\rho_{pol}{}^2(\phi_{pol}^{layer})^2 2\pi d_{pol} \qquad (10b)$$

Here ϕ_{wax}^{plate} and ϕ_{pol}^{plate} are the respective volume fractions of the wax and polymer plates in solution, $\Delta\rho_{wax}$ is the scattering contrast for wax, $\Delta\rho_{pol}$ is that for polymers, and ϕ_{wax}^{layer} and ϕ_{pol}^{layer} are the wax and polymer concentrations within the layers. In eq 10, they take care of the diluted scattering contrast as a consequence of the polymer or wax admixture, respectively. The

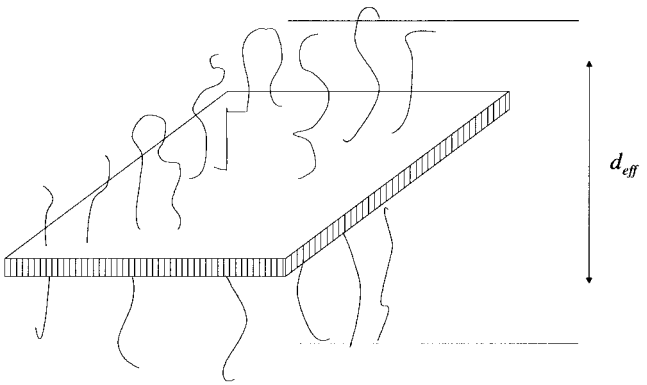

Figure 12. Schematic sketch of the polymer wax aggregates consisting from a monolayer of stretched C_{24} molecules crystallizing in a thin plate. Within the plate the polymers are incorporated forming a brush on both sides which leads to an homogeneous polymer platelet of thickness d_{pol}.

volume fraction of the plates is related to the overall volume fraction of wax or polymer by

$$\phi^{plate} = (\phi - \phi^{sol})/\phi^{layer} \tag{11}$$

Thereby, ϕ^{sol} stands for the solubilized fraction of the polymer or wax, respectively. Considering the experimentally observed homogeneous polymer distribution (Figure 8) across the layer, we approximately have

$$\phi_{pol}^{layer} = (1 - \phi_{wax}^{layer}) \tag{12}$$

The plate structures are jointly built from wax and polymer. Therefore, the volume fractions of the wax and polymer plates are related to each other by

$$\phi_{pol}^{plate} = \phi_{wax}^{plate}(d_{pol}/d_{wax}) \tag{13}$$

Using eqs 11−13, we now may rewrite eq 10a and 10b

$$\left.\frac{d\Sigma}{d\Omega}Q^2\right|_{wax} = \phi_{wax}^{plate}\Delta\rho_{wax}{}^2(\phi_{wax}^{layer})^2 2\pi d_{wax} \tag{14a}$$

$$\left.\frac{d\Sigma}{d\Omega}\right|_{pol} = \phi_{wax}^{plate}(d_{pol}/d_{wax})\Delta\rho_{pol}{}^2(1 - \phi_{wax}^{layer})^2 2\pi d_{pol} \tag{14b}$$

with the measured forward scattering (see Tables 4 and 5), the known contrast factors (see Table 1), and the measured thicknesses; eq 14a and 14b may be used together with eqs 11−13 to calculate the volume fractions of polymer and wax within the platelets as well as total aggregated volume fractions $\phi^{plate}\phi^{layer}$. The results are displayed in Table 6. Finally, the platelet area per cubic centimeter may be evaluated from $A_{wax}/V = \phi_{wax}^{plate}/d_{wax}$. The evaluated platelet areas are also given in Table 6.

Figure 13 displays the temperature dependence of the aggregated polymer and wax volume fractions for the $\phi_{wax} = 0.005$ and $\phi_{wax} = 0.01$ samples. Both samples contained the same volume fraction of $\phi_{pol} = 0.01$ polymer. As may be seen in both cases polymer and wax aggregation runs in parallel to each other signifying again, the cocrystallization process.

Exploiting eq 7, we may estimate the average size of the 3-d crystals formed. We take the results of the $\phi_{wax} = 0.02$ sample at $T = -22$ °C as an example. With $\phi_{wax}^{sol} \cong 0.0025$ (Table 6) and about $\phi_{wax} = 0.0043$ within the plate structures, the 3-d crystal volume fraction amounts to $\phi_{wax}^{cryst} \cong 0.0132$. For the surface to volume ratio S/V, eq 7 then gives $S/V = 2.57 \times 10^5$ cm^2/cm^3. With the assumption of spherical-like crystallites we find an average size of $a \cong 2400$ Å. The crystal size obtained in this manner is compatible with the observation of the asymptotic Porod scattering in our range of observation: $Q_{min}a = 5 \gg 1$.

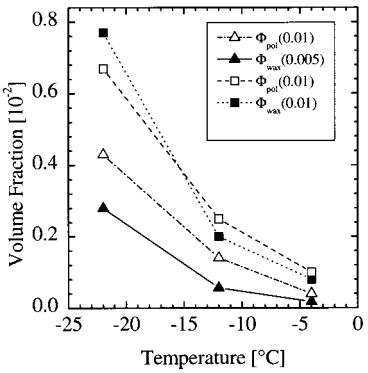

Figure 13. Temperature dependence of the aggregated volume fractions of wax and polymer at $\phi_{pol} = 0.01$ and $\phi_{wax} = 0.005$ (△, ▲) and $\phi_{pol} = 0.01$ and $\phi_{wax} = 0.01$ (□, ■).

We now address the question, whether the 3-d objects grow independently from the polymer mediated plate structures or whether the polymer/wax plates nucleate the 3-d crystal growth. Qualitatively, the scattering data may be interpreted in both directions. A more quantitative look, however, favors polymer wax platelet as nucleators for the 3-d wax crystals.

1. The polymer structures themselves are always 2-dimensional or at least very close to it (see Figures 4 to 7).

2. Wax and polymer appear to form plates only if $\phi_{wax} \leq \phi_{pol}$.

3. If $\phi_{wax} > \phi_{pol}$, a large number of little crystals with a large surface-to-volume ratio are nucleated, thus already indicating the nucleation function of the primary polymer wax platelets.

4. A close inspection of the polymer scattering traces from the $\phi_{wax} = 0.02$ samples under polymer contrast in Figure 7 shows that the power law indices α are larger than 2, indicating an admixture of 3-d structures to the polymer scattering. Thus, the polymers to some extent take part in the 3-d structures.

5. If we assume that the polymer would only cocrystallize with the wax into plates and that the rest of the wax crystallizes independently, then, according to Table 6 at $\phi_{wax} = 0.02$, the amount of polymer included in the aggregates would be reduced from $\phi_{pol} = 0.0067$ at $\phi_{wax} = 0.01$ to $\phi_{pol} = 0.005$ at $\phi_{wax} = 0.02$.

6. Finally, the morphology of the wax aggregate changes profoundly in the presence of polymers even if the wax concentration exceeds the polymer concentration by large amounts.[3]

These facts together indicate strongly that we are dealing with a staged mechanism where polymer and wax form 2-d platelets which then nucleate 3-d wax crystals. Thus, one may anticipate that these polymers will act as flow improvers for waxy crude oils.[10]

V. Conclusions

The experiments on the mixed aggregation of partially crystallizable PEB-11 and wax in decane solution have unraveled a highly interesting cocrystallization process. In the presence of wax, the polymers cocrystallize with the wax in thin sheets consisting of a single paraffin

Table 6. Aggregation Parameters

	ϕ_{wax}	ϕ_{wax}^{layer}	$\phi_{wax}^{plate}\phi_{wax}^{layer}$	ϕ_{pol}^{layer}	$\phi_{pol}^{plate}\phi_{pol}^{layer}$	area plate (10^4 cm^2/cm^3)	area/ϕ_{wax} (10^6 cm^2/cm^3)
$T = -22$ °C	0.005	0.76	0.0028	0.24	0.0043	1.22	2.25
	0.01	0.87	0.0077	0.153	0.0067	2.94	2.75
	0.02[a]	0.81	0.0043	0.19	0.005	1.77	0.78
$T = -12$ °C	0.005	0.62	0.000 53	0.38	0.0014	0.31	0.56
	0.01	0.78	0.002	0.22	0.0025	0.85	0.77
	0.02[a]	0.83	0.002 84	0.17	0.001 94	1.14	0.56
$T = -4$ °C	0.005	0.55	0.000 17	0.45	0.0004	0.10	0.16
	0.01	0.69	0.008	0.31	0.001	0.37	0.27
	0.02[a]	0.8	0.002	0.2	0.0015	0.86	0.41

[a] Aggregation parameters from the platelet fraction only.

layer surrounded by amorphous polymer hairs on both plate sides. Such structures have not been seen before. The polymer brush is thus very well-defined indicating a very homogeneous distribution of the polymer in the wax-stabilized plate. The polymer volume fractions in the brush are similar to those in the PE−PEP diblock systems. The conditions for the formation of these aggregates seem to be dictated by a very delicate balance between the enthalpy gain from the cocrystallization and the entropy loss from the conformation entropy of the polymer. The fact that the polymer prefers the cocrystalline state to that of self-aggregation indicates a preferential free energy situation, which could come from a relatively smaller entropy loss due to the paraffin process in the polymer-crystalline aggregates. It is conceivable that at lower temperatures these cocrystallized aggregates may emulate the self-assembled diblock copolymers and act as nucleators for shorter chain paraffin crystals.[2]

Varying the ethyl branch content of the polymer and possibly the molecular weight could allow a tuning of the aggregation process such that the polymer cocrystallizes with the largest paraffin in a fuel and then subsequently nucleates the lower paraffinic fractions. For such an optimization, systematic studies on the dependence of the aggregation process on PEB crystallinity and paraffin length are required. In particular, the thermodynamics of the process are in need of further understanding. Finally, we wish to note that the presence of the polymer arrests the 3-d growth of the layers. Hence, the act of cocrystallization of PEB-11 with the C_{24} paraffin creates brush-stabilized single layer paraffin crystals. This behavior may prove to be a viable mechanism regarding the development of flow improvers for waxy crude stocks.

References and Notes

(1) Richter, D.; Schneiders, D.; Monkenbusch, M.; Willner, L.; Fetters, L. J.; Huang, J. S.; Lin, M.; Mortenson, K.; Farago, B. *Macromolecules* **1997**, *30*, 1053.
(2) Leube, W.; Monkenbusch, M.; Schneiders, D.; Richter, D.; Adamson, D. A.; Fetters, L. J.; Dounis, P.; Lovegrove, R. *Energy Fuels* **2000**, *14*, 419.
(3) Ashbaugh, H. S.; Fetters, L. J.; Adamson, D. A.; Prud'homme, R. K. *J. Rheol.*, submitted for publication.
(4) Fetters, L. J.; Graessley, W. W.; Krishnamoorti, R.; Lohse, D. J. *Macromolecules* **1997**, *30*, 4973.
(5) Carella, J.; Graessley, W. W.; Fetters, L. J. *Macromolecules* **1984**, *17*, 2775.
(6) Schwahn, D.; Richter, D.; Wright, P. M.; Symon, C.; Fetters, L. J.; Lin, M. *Macromolecules* **2002**, *35*, 861.
(7) Morton, M.; Fetters, L. J. *Rubber Chem. Technol.* **1975**, *48*, 359.
(8) For neutron-scattering experiments at the FRJ-2 in Jülich see: www.neutronscattering.de.
(9) Brecevic, L.; Gorside, J. *J. Chem. Eng. Data* **1993**, *38*, 598.
(10) Ashbaugh, H. S.; Radulescu, A.; Prud'homme, R. K.; Schwahn, D.; Richter, D.; Fetters, L. J. *Macromolecules*, submitted.

MA0120456